applied sciences

MDPI

Article

Mesenchymal Stem Cell Differentiation Driven by Osteoinductive Bioactive Nanoscale Topographies

Catarina R. Pedrosa [1,2,3,4], Christel Chanseau [1,2,3], Christine Labrugère [5], Sivashankar Krishnamoorthy [4,*,†] and Marie-Christine Durrieu [1,2,3,*,†]

1 Chimie et Biologie des Membranes et Nano-Objets (UMR5248 CBMN), Université de Bordeaux, Allée Geoffroy Saint Hilaire-Bât 14, 33600 Pessac, France; catarinarpedrosa@gmail.com (C.R.P.); christel.chanseau@u-bordeaux.fr (C.C.)
2 CNRS, CBMN UMR5248, Allée Geoffroy Saint Hilaire-Bât 14, 33600 Pessac, France
3 Bordeaux INP, CBMN UMR5248, Allée Geoffroy Saint Hilaire-Bât 14, 33600 Pessac, France
4 Materials Research and Technology (MRT) Department, Luxembourg Institute of Science and Technology (LIST), 41 Rue du Brill, Belvaux, Luxembourg L-4422, Luxembourg
5 PLACAMAT, UMS3626, CNRS-Université de Bordeaux, 87 Avenue Docteur Albert Schweitzer, 33600 Pessac, France; Christine.LABRUGERE@placamat.cnrs.fr
* Correspondence: sivashankar.krishnamoorthy@list.lu (S.K.); marie-christine.durrieu@inserm.fr (M.-C.D.)
† Equally contribution.

Abstract: Human mesenchymal stem cells (hMSCs) respond to the characteristics of their surrounding microenvironment, i.e., their extracellular matrix (ECM). The possibility of mimicking the ECM offers the opportunity to elicit specific cell behaviors. The control of surface properties of a biomaterial at the scale level of the components of the ECM has the potential to effectively modulate cell response. Ordered nanoscale silicon pillar arrays were fabricated using reverse micelles of block copolymers on full wafers, with standard deviations lower than 15%. Bioactive synthetic peptides were covalently grafted on nanoarrays to evaluate possible synergies between chemistry and topography on osteogenic differentiation of hMSCs. Functionalization with RGD (Arg-Gly-Asp) and BMP-2 (bone morphogenetic protein-2) mimetic peptides lead to an enhancement of osteogenic differentiation. Bare nanopillar arrays of reduced pitch were found to promote faster hMSC differentiation. These findings highlight the relevance of investigating possibilities of engineering in vitro systems which can be fine-tuned according to the envisaged cell response.

Keywords: nanotopography; surface functionalization; mimetic peptide; mesenchymal stem cell; osteogenic differentiation

check for updates

Citation: Pedrosa, C.R.; Chanseau, C.; Labrugère, C.; Krishnamoorthy, S.; Durrieu, M.-C. Mesenchymal Stem Cell Differentiation Driven by Osteoinductive Bioactive Nanoscale Topographies. *Appl. Sci.* **2021**, *11*, 11209. https://doi.org/10.3390/app112311209

Academic Editors: Barbara Nebe and Karine Anselme

Received: 22 July 2021
Accepted: 9 November 2021
Published: 25 November 2021

Publisher's Note: MDPI stays neutral with regard to jurisdictional claims in published maps and institutional affiliations.

Copyright: © 2021 by the authors. Licensee MDPI, Basel, Switzerland. This article is an open access article distributed under the terms and conditions of the Creative Commons Attribution (CC BY) license (https://creativecommons.org/licenses/by/4.0/).

1. Introduction

Biomaterials can be engineered to improve and actively guide cell response in a controlled way [1]. To achieve that, material surfaces should be able to mimic the in vivo microenvironment to which a cell is normally in contact with, i.e., to mimic its extracellular matrix (ECM) [2]. Since most cell-ECM interactions occur at nanoscale (e.g., growth factor-receptor interaction), control of biomaterial surface properties at this scale level is of utmost importance. Most reported studies rely on the creation of micro-/nanoscale topographies, the fine-tuning of surface chemistry of a material or the tuning of the stiffness of materials for the cell type under investigation to perform such control [3–7]. Mesenchymal stem cells (hMSCs) have been one of the main cell types used in studies of modulation of cell fate through the control of materials design [4]. hMSC are easy to culture and manipulate in ex vivo culture and these cells are a very promising option for bone tissue engineering applications, due to their osteogenic differentiation potential (among the potential to differentiate into other lineages, namely adipogenic or chondrogenic) [8].

Nanofabrication methods commonly used in electronic applications grant powerful tools to produce nanoscale features which can be translated into platforms for cell-substrate

interaction studies. Though these fabrication methods can potentially be applied to a multitude of materials, state-of-art approaches are normally developed for silicon. Several variations of nanotopographies, namely pillars, rods, pits, and their organization on the surface (i.e., ordered/disordered) have been used in the investigation of hMSC differentiation towards osteoblastic lineage [3,7,9–13]. The pillar arrays are further, more stable configurations than rods attached to the surface via their long axis. There is no real consensus on which geometry is the most efficient on the promotion of osteogenesis [14]. Even studies investigating identical nanotopographies can report contradictory results [5,15]. Material topography is a very powerful parameter for the control of cell behavior, but it is necessary to keep in mind that any slight change of chemistry, at the level of material surface or of culture media composition, besides cell origin (e.g., adipose-/bone marrow-derived hMSCs, donor age) can have an impact on cell response of the same amplitude as topography [4,16–18]. We reported that osteogenic differentiation of hMSCs on silicon nanopillar arrays is enhanced when cells are cultured on nanopillars of larger diameter (100 nm) and height (80 nm) [18]. It was observed that depending on the age of the donor, osteogenic differentiation was further enhanced for smaller or larger spacing between features (140–200 nm) for younger and older donors. Our earlier work had focused on the impact of nanotopographies without chemical factors immobilized onto the silicon surfaces. Our efforts in the current work are however directed at the impact of surface chemistry due to introduction of BMP and RGD (Arg-Gly-Asp) peptides on the nanotopographies that can independently control the response of the hMSCs.

Molecules of varied sizes, ranging from full-length ECM proteins to short linear peptides have been investigated as possible ways of assigning bioactivity to a material surface [4,19–25]. Although the use of full-length ECM proteins has proven to be a successful way of controlling cell behavior on bioactive materials, their use is hindered due to intrinsic limitations (e.g., poor stability, safety concerns) [19]. To overcome these shortcomings, synthetic peptides encompassing only the amino acids (aa) necessary to support a particular biological activity have been investigated [20,26]. Mimetic peptides can be synthesized with high purity, lower costs, and specific active sites can be engineered in a controlled way [19]. Moreover, contrary to proteins, conformation and density of short molecules can be controlled when bound to a material [19]. The most representative motif used for the improvement of cell adhesion is the sequence of aa arginine-glycine-aspartic (RGD), which in vivo mediates the binding of ECM proteins (e.g., fibronectin) to transmembrane integrin receptors [27–29]. The growth factors most commonly used for the enhancement of osteogenic differentiation of hMSCs are bone morphogenetic proteins (BMPs), particularly BMP-2 [30,31]. Most studies take advantage of only the sequence responsible for the osteogenic activity of this molecule to functionalize biomaterials for bone tissue engineering applications [19,32,33]. The combination of a peptide promoting cell adhesion with one promoting cell differentiation for the co-functionalization of a biomaterial has been reported to further enhance differentiation when compared with the grafting of only one peptide sequence, such as a BMP-2 mimetic peptide [34–38]. Several studies can be found reporting also synergistic effects of combining nanotopographies with chemical cues on osteogenic differentiation of hMSCs or osteoblast progenitors [39–41].

Guided by these considerations, this study aims at investigating osteogenic differentiation of hMSCs cultured on Si nanopillar arrays functionalized with RGD peptide and/or a BMP-2 mimetic peptide and comparing it with the hMSC response on bare un-functionalized counterparts. The peptide immobilization strategy involves the grafting of an amino functional organosilane to the silicon surface and changing the terminal amine to a maleimide-functional surface by coupling a heterobifunctional crosslinker. The maleimideterminated surfaces then are coupled with a peptide through the thiol group on the terminal cysteine of the peptide. Geometry of the arrays was defined according to Pedrosa et al. [18]. The prepared surfaces were carefully characterized by atomic force microscopy (AFM), scanning electron microscopy (SEM) and X-ray photoelectron spectroscopy (XPS). To evaluate to which extent hMSC differentiation was promoted, expression

of early (runt-related transcription factor 2, Runx2, and collagen type I, Col1A1) and late (osteopontin, OPN, and osteocalcin, OCN) osteogenic differentiation markers [34,36] was investigated by immunofluorescence and quantitative polymerase chain reaction (RT-qPCR).

2. Materials and Methods

Materials: Polystyrene-block-ptranscipoly (2-vinylpyridine) (PS-b-P2VP) (M_w 248,000-b-195,000 g mol^{-1}, polydispersity index 1.08) was purchased from Polymer Source (Toronto, ON, Canada) and used without further purification. All solvents, acids and bases were purchased from Sigma Aldrich (Saint-Quentin-Fallavier, France), unless stated otherwise. Prime grade silicon wafers with 25 nm thick thermally grown SiO_2 film were acquired from Siegert Wafer (Aachen, Germany). The 3-aminopropyltriethoxysilane (APTES) and 3-succinimidyl-3-maleimidopropionate (SMP) were purchased from Sigma Aldrich. Peptides used for surface functionalization (GRGDSPC, afterwards designated as RGD peptide, and KRKIPKASSVPTELSAISMLYLC, afterwards designated as BMP-2 mimetic peptide) were synthesized by Genecust (Luxembourg). Bone marrow-derived human mesenchymal stem cells (hMSCs) were acquired from PromoCell (Heidelberg, Germany). Basal culture medium αMEM and fetal bovine serum (FBS) were purchased from Gibco, ThermoFisher Scientific (Bordeaux, France). All reagents used in DNA digestion and RNA retrotranscription were acquired from ThermoFisher Scientific. Thermo Scientific Maxima Reverse Transcriptase (Thermo Scientific, Illkirch-Graffenstaden, France) and Primers (Thermo Scientific) used for RT-qPCR were acquired. SsoAdvanced™ Universal SYBR® Green Supermix was purchased from Bio-Rad (Hercules, CA, USA). Bovine serum albumin (BSA) and sample mounting media with DAPI (Fluoroshield™ with DAPI) were purchased from Sigma-Aldrich. Primary antibody against runt-related transcription factor 2 (Runx2, rabbit monoclonal) was purchased from Cell Signaling Technology Europe (Leiden, The Netherlands) (Ref: 12556S) and the primary antibody against osteopontin (OPN, mouse monoclonal) from Santa Cruz Biotechnology (Dallas, TX, USA) (Ref: sc-21742). Secondary antibodies were acquired from Invitrogen (Waltham, MA, USA), ThermoFisher Scientific.

2.1. Nanopillar Fabrication

Oxygen plasma reactive ion etching (RIE, PlasmaTherm 790 RIE, Saint Petersburg, FL, USA) at low bias was used for removal of organic contamination from the substrates, followed by CO_2 snow jet cleaning to remove any remaining small sized particles. Silicon nanopillar arrays were prepared according to the protocols described by Krishnamoorthy et al. [42] and Pedrosa et al. [18]. PS-b-P2VP was dissolved in anhydrous m-Xylene at a concentration of 0.5 wt% and stirred for 24 h. The reverse micelles obtained were spin-coated on clean wafers at 2000 or 5000 rpm to produce polymer templates distinct periodicities. Samples were afterwards subjected to brief Ar/O_2 plasma descumming (18 sccm Ar/2 sccm O_2, 4 mTorr, 4 W), and subsequently transferred into the oxide layer by CHF_3/Ar (12 sccm CHF_3/38 sccm Ar, at −90 °C, 30 mTorr, 200 W) and then into silicon by SF_6/O_2 plasma (50 sccm SF_6/10 sccm O_2, 10 mTorr, 25 W). Remaining silica was removed by wet etching with hydrofluoric acid (2% v/v). After each step, samples were characterized in detail by AFM (Innova, Bruker, MA, USA) and SEM (FIB-SEM, Helios 650, FEI Company, Laussane, Switzerland). Nanopatterned wafers were diced in 1 cm^2 chips for easier utilization in cell culture.

2.2. Surface Biofunctionalization

Surfaces were activated in solutions of hydrogen peroxide (30 wt%) and sulfuric acid at a ratio 1:4 for 30 min. Samples were consecutively sonicated in deionized water. Surface functionalization protocol, based on the work of Porté-Durrieu et al., is schematically represented in Figure 1a [27]. Immediately after surface activation, samples were degassed for 15 h under high vacuum (10^{-5} mbar) at 150 °C. This treatment was followed by a silanization step under an inert atmosphere using a solution of APTES 2% (v/v) in anhydrous hexane for 3 h at room temperature (RT). Samples were sonicated in anhydrous hexane to

remove silane molecules in excess, and cured for 2 h under high vacuum (10^{-5} mbar) at 100 °C. Amine-terminated surfaces were conjugated with the SMP crosslinker (4 mM) in dimethylformamide (DMF) for 3 h at RT. The succinimidyl group of SMP can react with amine groups on the surface, leaving the maleimidyl group available for the reaction of the thiol group of the cysteine included at the end of the sequence of both peptides. Afterwards, samples were sonicated in DMF to remove SMP molecules in excess, and dried for 2 h under high vacuum (10^{-5} mbar) at 70 °C. Finally, RGD peptide, BMP-2 mimetic peptide or a combination of both peptides at a ratio 1:1 was immobilized on the surfaces [30–32,34] at RT. Samples were incubated for 24 h with solutions of peptides at 0.1 mM in deionized water. Samples were afterwards sonicated in deionized water to remove unbound peptides and stored in phosphate buffered saline (PBS).

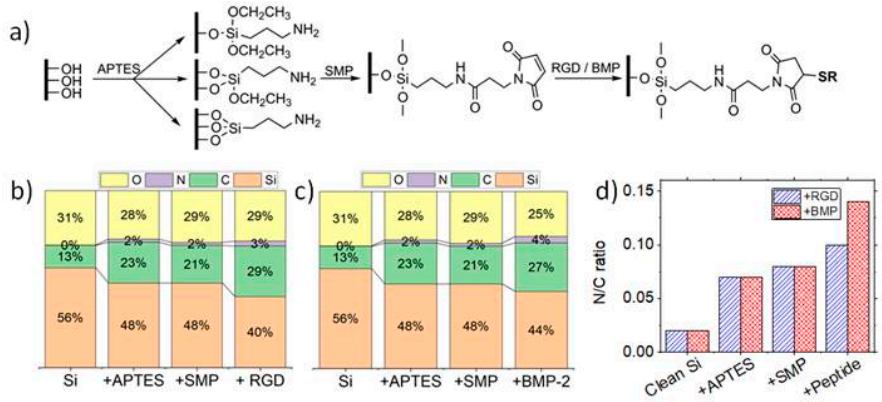

Figure 1. (**a**) Schematic representation of surface functionalization process. R represents the peptide of interest bound to the crosslinker SMP. This selective binding occurs between the maleimidyl group of the crosslinker and the thiol group only available in the cysteine (for both peptides). (**b**–**d**) chemical surface composition determined by XPS (**b**,**c**) stacked column plots show changes in elemental composition with each step of surface functionalization expressed as relative changes to the Si, C, N and O for (**b**) RGD or (**c**) BMP-2 peptides and (**d**) evolution of N/C ratios corresponding to each step of grafting on flat silicon surfaces.

2.3. XPS Characterization

Samples were characterized by XPS before and after surface modification and after each functionalization step to confirm that the reactions were successful. XPS was performed (K-Alpha, ThermoFisher Scientific) with a monochromated AlKα source at 100 W with spot size of 400 µm. For each condition, five regions were analyzed to confirm the uniformity of the treatment across the whole surface.

2.4. Cell Culture

Nanostructured chips were disinfected in 70% ethanol overnight prior to their use in cell culture. Human mesenchymal stem cells (hMSCs) from bone marrow (one donor of 65 years old) were purchased from PromoCell (Heidelberg, Germany) (C-12974). The hMSCs are positive for CD73, CD90, and CD105 expression, and are negative for CD34, CD45, CD14, CD19, CD11b, CD79α and HLA-DR. Bone marrow hMSCs were seeded at passage five at an initial density of 10^4 cells/cm^2 on the samples. Cells were seeded in serum-free medium (α-MEM medium-(Fisher ref: 1071214)) to ensure cell interaction directly to the material, and incubated at 37 °C, 5% CO_2. After 4 h, medium was changed to αMEM completed with 10% FBS, afterwards referred as basal medium. Culture medium was replaced twice a week. hMSCs were cultured for 2 weeks [43].

2.5. Immunofluorescence Assays

Immunostaining was performed after 2 weeks of cell culture to investigate the expression of the selected osteogenic markers. Cells were fixed with paraformaldehyde (4% v/v) in PBS (neutral pH), permeabilized with ice-cold methanol and Triton-X 100

(0.5% v/v). Samples were subsequently incubated with BSA (1% v/v) to avoid possible non-specific interactions. Samples were incubated with the primary antibodies against Runx2 (1/1600, ref: 12556S, Cell Signaling Technology) and OPN (1/200, ref: sc-21742, Santa Cruz Biotechnology) for 1 h at 37 °C. After 3 washes with Tween-20 (0.05% v/v) (5 min each), samples were incubated for 1 h at 37 °C with the secondary antibodies goat anti-rabbit IgG coupled with AlexaFluor™ 488 (ref: A11008, Invitrogen) and goat anti-mouse IgG coupled with AlexaFluor™ 647 (refA21235, Invitrogen). Samples were washed with a solution of Tween-20 (three times five minutes) and mounted and counterstained with DAPI. Fluorescence microscopy (Leica microsystem DM5500B, microscope with a motorized, programmable stage using a CoolSnap HQ camera controlled by Metamorph software) was used. Image J software was used to quantify the relative fluorescence intensity. Fluorescence intensity measurements of Runx2 and OPN were performed for $n = 3$, considering the expressions of at least 100 cells per each type of surface. As principally expressed in nucleus, only nuclear fluorescence signal was analyzed since both Runx2 and OPN are expressed inside cell nucleus [18,36,44–46]. Nuclei were delimited using DAPI signal to define regions of interest. Background was determined as the signal obtained from cells stained only with secondary antibody, and subtracted from the fluorescence measured from cells marked with primary and secondary antibodies. Fluorescence results for each condition were presented as average fluorescence intensity and standard deviation.

2.6. RT q-PCR

Total RNA from hMSC cultured for 2 weeks was isolated using RNeasy Mini Kit, genomic DNA was removed using TURBO DNA-free kit. Total RNA was quantified using spectrophotometer NanoDrop 1000 (ThermoFisher Scientific) and RNA integrity was evaluated using an Agilent bioanalyzer 2100 with an RNA 6000 Nano kit (Agilent, Santa Clara, CA, USA) (RIN values from 7 to 10). cDNA was synthesized from 500 ng of total RNA with the help of random primers and Maxima Reverse Transcriptase. RNA retrotranscription reaction was performed in two steps: incubation at 50 °C for 1 h, and subsequent incubation at 72 °C for 15 min. Aliquots of cDNA underwent dye-based RT-qPCR for the study of three genes expressed during osteoblastic differentiation (primers listed in Table 1). RT-qPCR was performed using 4 ng of cDNA, and primers at a concentration of 500 nM, for a final volume of 10 µL. RT-qPCR was performed using a CFX Connect™ Real-Time PCR System (Bio-Rad), using 2 genes of reference: RPC53 and PPIA. Forty PCR amplification cycles were performed for each experiment, consisting of incubating the solution at 95 °C for 5 s, followed by an incubation at 60 °C for 10 s. Cq for the genes of interest were normalized against the reference genes selected using the software BestKeeper: PPIA and RPC [24,34,47]. Relative expression levels were calculated using the comparative method (ΔΔCq).

Table 1. Primers used for RT-qPCR.

Gene (Protein)	Primer Sequence
POLR3D (RPC53)	5′-ACCCTGGCTGACCTGACAGA-3′ (Forward)
	5′-AGGAGTTGCACCCTTCCAGA-3′ (Reverse)
PPIA (PPIase A)	5′-CGGGTCCTGGCATCTTGT-3′ (Forward)
	5′-CAGTCTTGGCAGTGCAGATGA-3′ (Reverse)
RUNX2 (Runx2)	5′-AAGTGCGGTGCAAACTTTCT-3′ (Forward)
	5′-TCTCGGTGGCTGGTAGTGA-3′ (Reverse)
COL1A1 (COLIA1)	5′-ACATGTTCAGCTTTGTGGACC-3′ (Forward)
	5′-TGATTGGTGGGATGTCTTCGT-3′ (Reverse)
BGLAP (OCN)	5′-GACTGTGACGAGTTGGCTGA-3′ (Forward)
	5′-CTGGAGAGGAGCAGAACTGG-3′ (Reverse)

Gene expression was normalized using flat silicon sample as control. For each condition, two replicates were considered.

2.7. Statistical Analysis

Data are expressed as mean ± standard error, except if stated otherwise and analyzed by one-way analysis of variance (ANOVA) and Tukey's test for multiple comparisons. Statistical analyses were performed using CFX Maestro Software (Bio-Rad, USA) for RT-qPCR data and GraphPad Prism (San Diego, CA, USA) for immunofluorescence. Significant differences were determined for p values ≤ 0.05. * $p \leq 0.05$, ** $p \leq 0.01$, and *** $p \leq 0.001$.

3. Results

3.1. Preparation of Bioactive Nanostructured Samples

Silicon nanopillars were fabricated on full wafers with high uniformity and reproducibility. Such characteristics were made possible due to the ability of PS-b-P2VP to self-assemble into polymeric colloids able to further organize into hexagonally distributed templates, as reported by Krishnamoorthy et al. [42]. Solutions of reverse micelles were spin-coated on the substrates at two distinct speeds to prepare polymeric templates of identical diameter, but different periodicity, as summarized in Table 2. The SiO_2 thin film was used as an intermediate mask to improve the geometric characteristics of the nanopillars, given its superior selectivity for Si etching than the initial block copolymer (BCP) film, while preserving the dimensions of the initial reverse micelles. SEM characterization (Figure 2) demonstrated that feature heights were close to the 80 nm targeted (Table 2). The success of the surface modification was confirmed by XPS after each step on flat silicon substrates (Figures 1 and 3) and extrapolated to the nanostructured samples, considering the chemical composition observed before and after peptide grafting. High resolution spectra for C1s and N1s at each step of surface functionalization are represented in Figure 3.

Table 2. Characteristic dimensions of the nanopillar arrays determined by AFM and SEM. (For easier understanding of subsequent results, nanoarrays were labeled as A and B).

Label	Spin Speed/rpm	Diameter/nm	Periodicity/nm	Height/nm
A	2000	105 ± 14	141 ± 12	75 ± 6
B	5000	104 ± 13	201 ± 23	82 ± 6

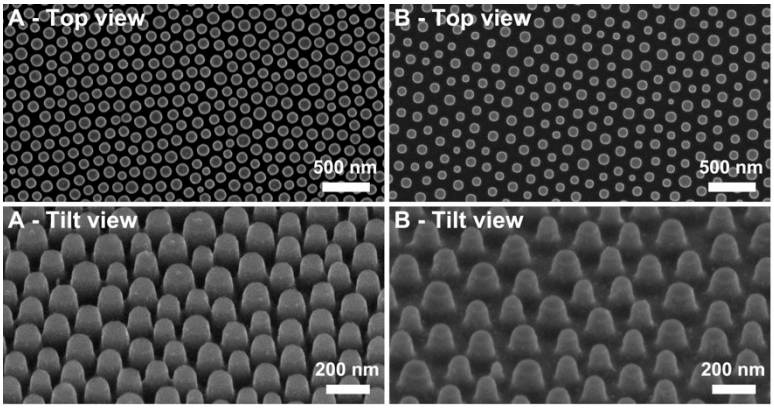

Figure 2. SEM images of the fabricated nanopillars at top and tilted views of nanostructures labelled as (**A**) and (**B**) as presented in Table 2.

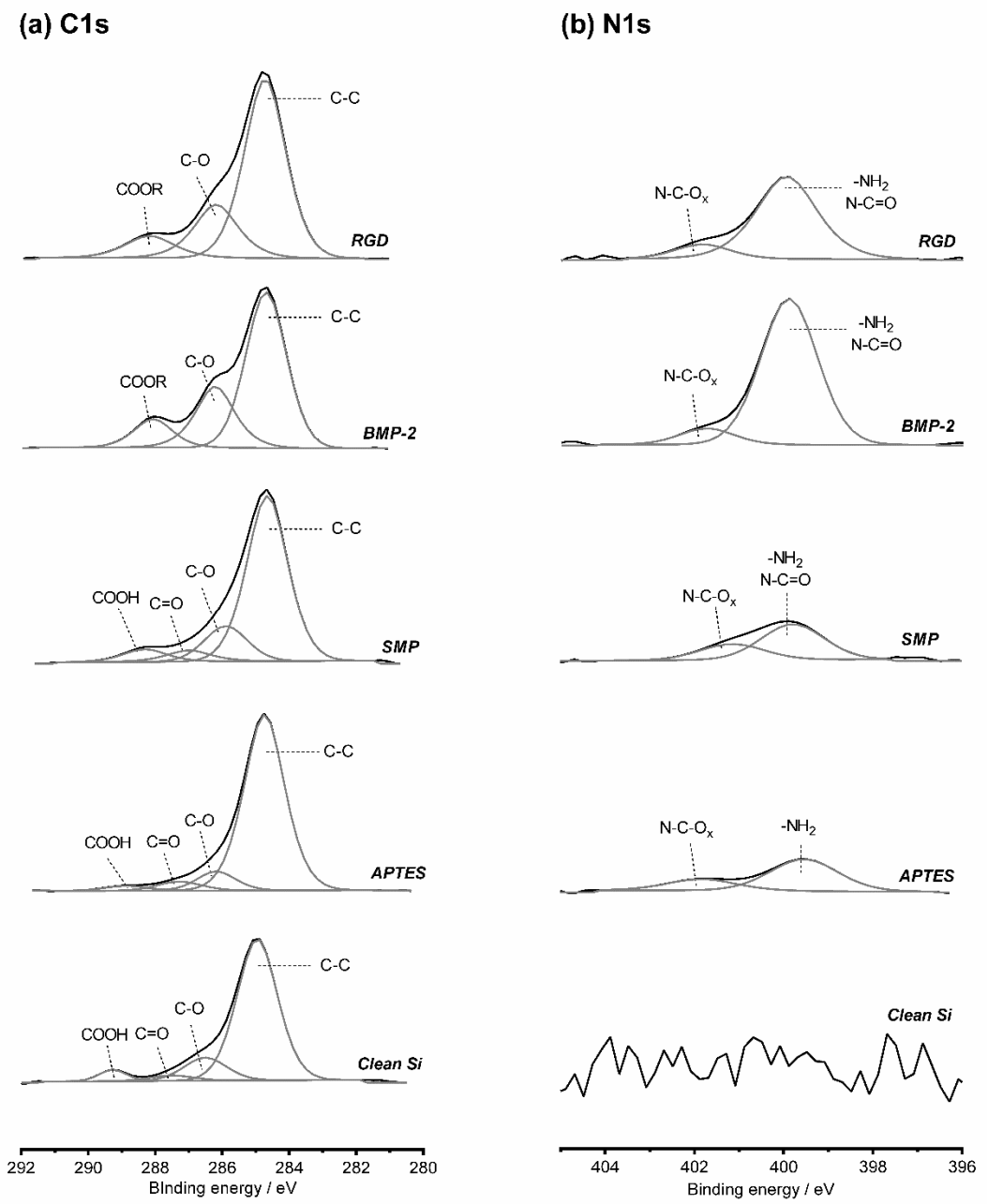

Figure 3. Deconvolution of high resolution XPS spectra of C1s (**a**) and N1s (**b**) at each step of surface functionalization, namely, Si (control), APTES, SMP followed by grafting of RGD or BMP-2 on flat silicon with values as shown in Figure 1.

Silicon substrates characterized before functionalization exhibited high silicon (56.4%) and oxygen (30.8%) percentages, characteristic of the native silicon oxide layer of the substrates. A slight carbon contamination (12.6%) is impossible to avoid, even if the samples were only exposed to air during mounting on XPS sample holder. Still, this value was within the same set of values reported in previous studies, therefore being in an acceptable range [2,27,35]. Nitrogen content was 0.2%, a value corresponding to measurements at the detection limits of the XPS system. After silanization, XPS surveys showed a decrease in silicon content (to 47.8%), a significant increase in carbon content (to 23.0%) and the appearance of nitrogen (1.7%) associated with the formation of an APTES layer on the surface. High resolution C1s spectrum indicated an increase in C-C bonds compared with the clean substrate. NH_2-C bonds were observed in N1s high resolution spectrum, confirming the existence of the silane layer on the treated samples. The slight increase of oxygen (to 29.3%) after reaction of the amine-terminated surfaces with SMP

indicates the presence of the crosslinker on the surfaces. Nitrogen remained constant after binding of SMP, which can be a consequence of the existence of only one nitrogen atom in a SMP molecule, which is not sufficient to contribute to a change in the overall percentages of elemental composition. A minor decrease in carbon content was verified, even if each crosslinker molecule has seven carbon atoms. This fact may be related with a reduced carbon contamination on the new surfaces than on silanized surfaces.

Finally, peptides were bound to the maleimide group of SMP crosslinker via their cysteine. The significant decrease on silicon content observed after BMP-2 binding can be associated with the large dimensions of this molecule, preventing the possibility of interactions of the X-rays with the silicon substrate. An increase in carbon (to 27.4%) and nitrogen content (to 3.7%) are also linked to the immobilization of the mimetic peptide which is constituted by a large number of carbon and nitrogen atoms. Additionally, high resolution C1s spectra shows an increase in C-C bonds. The significant increase of N-C=O alongside with the appearance of N-C=Ox of higher energy in the high resolution N1s spectrum, further confirms the immobilization of the BMP-2 mimetic peptide on the surface. A similar tendency was detected after the grafting of RGD peptide. It is worth noting the reduced standard deviations observed in all measurements, confirming the uniformity of immobilization of the molecules on the surfaces.

Since cells are rather sensitive to surface chemistry, it was also necessary to infer whether the different topographies present a similar chemistry after surface functionalization. Therefore, XPS spectra for the three topographies were deconvoluted and compared before and after peptide grafting (Table 3). Similar results were observed concerning surface functionalization with RGD. Regarding Si2p spectra, all samples showed a substantial decrease in Si^0 substrate component, associated with the immobilization of large-sized molecules, as BMP-2 mimetic peptide. Surface functionalization leads to an increase in the amount of C-C bonds in the C1s spectra of all samples, and to a slight increase of C-O bonds. Plain samples exhibited the characteristic COOH groups, which reacted with APTES, not being detected after surface modification on any sample.

Table 3. Atomic percentages obtained from deconvolution of high resolution XPS spectra after sample cleaning (clean) and after BMP-2 grafting (BMP-2) for the flat control (F) and the nanostructured Samples A and B. (Atomic % represented as % of total peak area).

	Bond	Atomic %					
		F		A		B	
		Clean	BMP-2	Clean	BMP-2	Clean	BMP-2
Si	Si^0	50.3	39.1	41.6	33.5	45.5	32.9
	$SiOC_3$	2.1	2.3	3.4	4.1	1.8	4.0
	SiO_2C_2, SiO_3C	5.6	5.2	7.7	5.2	8.3	4.6
C	C-C	10.3	16.8	14.4	19.1	12.0	19.6
	C-O	3.2	5.3	3.3	5.1	3.0	6.1
	COOR	0.0	3.7	0.0	3.2	0.0	3.6
	COOH	0.6	0.0	0.7	0.0	0.5	0.0
N	NH_2-C, N-C=O	0.0	3.2	0.0	3.0	0.0	2.9
	N-C-O_x	0.3	0.2	0.2	0.4	0.3	0.5
O	O=C	0.4	6.5	0.3	4.7	0.0	6.0
	O-C	27.3	17.7	28.4	21.7	28.5	19.9

3.2. Immunofluorescence Assays

After two weeks of culture on the selected nanostructures either plain or functionalized with RGD or/and BMP-2 mimetic peptide, hMSCs were fixed and immunostained to investigate the expression of Runx2 and OPN by immunofluorescence (Figure 4).

It was observed that, independent of the surface chemistry (RGD or/and BMP-2 functionalization), Runx2 expression was higher on Nanotopography A (pillars with reduced spacing). Regarding flat silicon surfaces, it was observed that expression of Runx2 could be enhanced if the substrate was functionalized with RGD peptide or, to a lesser extent, co-functionalized with both peptides. Still, for all cases the fluorescence signal detected on

flat samples was approximately half the signal observed on nanoarrays of Type A. Runx2 expression on bare B nanotopographies was similar to the level observed on plain flat surfaces. The same was noticeable for Surface B grafted with RGD peptide and flat modified with this peptide. Yet, grafting of BMP-2 mimetic peptide or the combination of the two peptides lead to a significant increase in expression of Runx2 on Nanostructures B (2-fold). Runx2 with Silicon with Nanopillars A (diameter 105 ± 14 nm, periodicity 141 ± 12 nm, height 75 ± 6 nm) with or without peptide functionalization is clearly overexpressed in comparison with flat silicon and silicon with Nanopillars B.

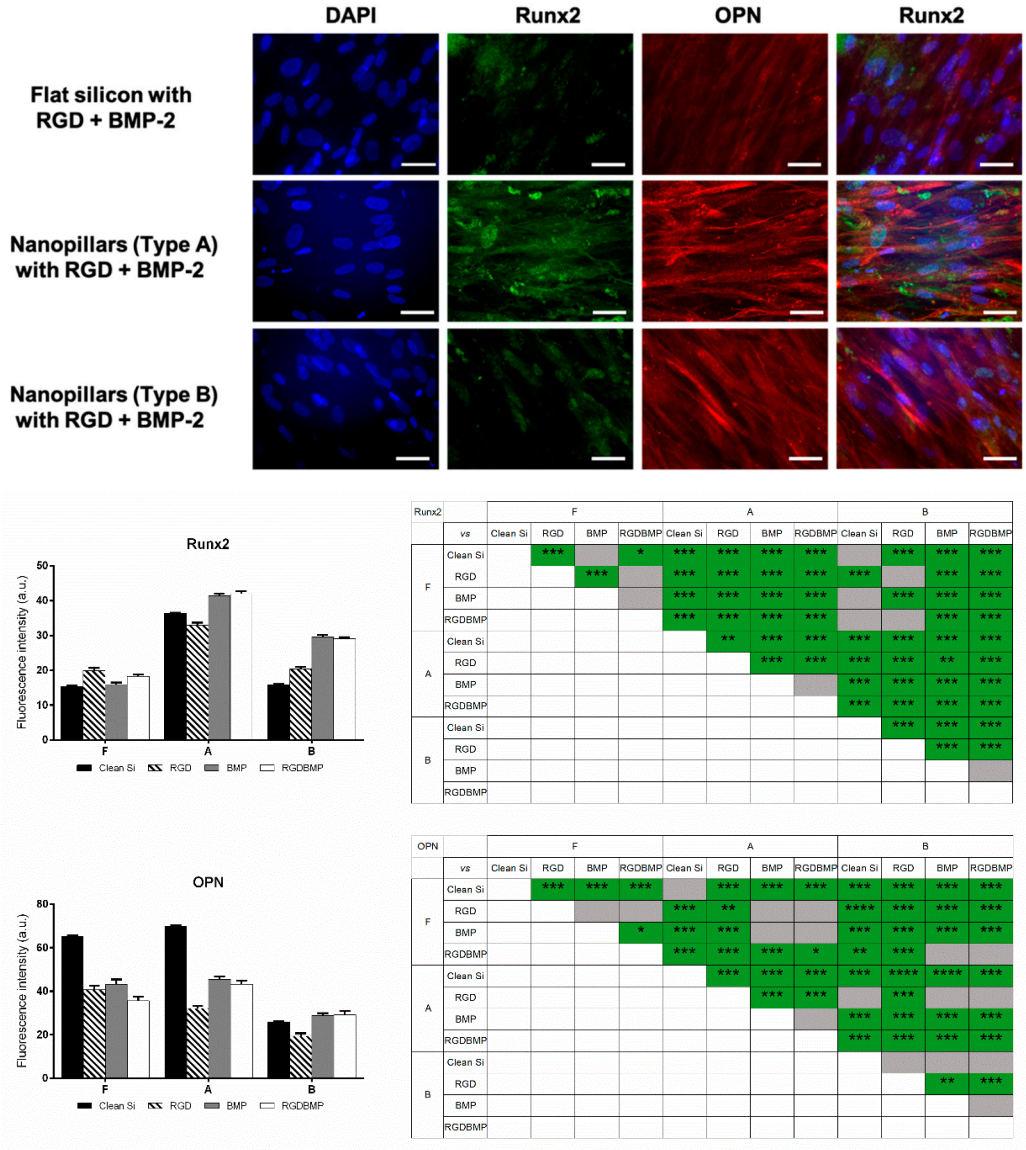

Figure 4. hMSCs cultured for 2 weeks on flat silicon (F) and silicon with Nanopillars A and B (Table 2) before and after functionalization with RGD and/or BMP-2 peptides (RGD alone, BMP-2 alone or combined RGD/BMP-2 peptides). Cells were stained for the early osteogenic (Runx2) marker in green, the late osteogenic (OPN) marker in red and cell nucleus in blue. An example is given here with RGD + BMP-2 peptides immobilization (**above**) (scale bar: 40µm). Quantitative analyses of the nuclei immunofluorescence intensity of Runx2 and OPN in hMSCs (**left**). Tables (**right**) summarize significant differences between conditions (grey: non-significant, green: significant differences. * represents $p < 0.05$, ** $p < 0.01$, *** $p < 0.001$).

Lastly, N-C=O components could be observed on all samples in C1s and in N1s spectra, further indicating that BMP-2 mimetic peptide was immobilized on the surfaces. Contrarily, OPN expression appeared to be dependent not only on the topography but also strongly on

surface chemistry, with higher fluorescence signal being detected on non-modified flat and on nanopillars with reduced pitch (Condition A). The change of surface chemistry of these two topographies (flat and Nanoarray A), achieved via peptide grafting induced a decrease in OPN expression to roughly two thirds of the signal on plain surfaces. Such decrease was notably evident for the Nanoarray A modified with RGD peptide. OPN expression on Topography B was rather low for all conditions (bare/functionalized).

3.3. RT-qPCR Assays

After two weeks of cell culture, total RNA was extracted, and RT-qPCR was performed to investigate the expression of the selected markers. Considering the large number of conditions to be compared, for each gene, results were normalized to a flat, bare silicon control. Hence, differences between nanotopographies and/or surface modifications can be easily distinguished. These results are summarized in Figure 5. It is interesting to note that similar levels of gene expression could be obtained on all topographies when RGD peptide and BMP-2 mimetic peptide were co-immobilized on the surfaces, and that such level of expression was the maximum observed. For the case of non-functionalized surfaces, Nanostructures A appeared to be the most relevant for promotion of osteogenic differentiation of hMSCs, as the highest expression levels for the genes studied was observed for this pattern. In particular, the expression of the three markers on nanopillars of Type A was significantly higher than their expression on flat substrates (as high as four-fold in the case of Runx2). Functionalization with RGD peptide caused an increase in expression, especially of the early differentiation marker Runx2. COL1A1 and OCN levels suffered a significant increase on flat surfaces after functionalization. Yet, for the other topographies, OCN expression did not change significantly.

BMP-2 mimetic peptide grafting had distinct effects on gene expression on each topology. Regarding Runx2 expression, it caused a significant increase in expression for cells cultured on flat samples (comparing with no modification or grafting of RGD peptide). However, Runx2 expression on Nanostructures A was similar to the one observed after functionalization with RGD peptide. Oppositely, BMP-2 functionalization on B samples lead to a significant decrease of Runx2 expression compared with RGD functionalization. The impact of BMP-2 on the remaining markers was rather different. Expression of COL1A1 and OCN was not as increased on all topographies as observed for Runx2 after surface functionalization with BMP-2 mimetic peptide. COL1A1 expression on cells cultured on A structures with BMP-2 peptide was even significantly lower than Bare A, or A grafted with RGD peptide. Oppositely, a significant increase in expression of COL1A1 was observed on B topographies.

Finally, co-immobilization of the two molecules had a positive impact on all topographies. Concerning flat surfaces, a significant increase on expression of all markers was noticeable when comparing with bare surfaces (14-fold for Runx2, 1.5-fold for COL1A1, 2-fold for OCN). However, gene expression of flat surfaces grafted with RGD and/or BMP-2 mimetic peptide did not show significant differences between themselves. The same tendency was observed for Nanotopography B with the diameter 104 ± 13 nm, the periodicity 201 ± 23 nm and height 82 ± 6 nm. Contrarily, gene expression of cells cultured on Topography A (diameter 105 ± 14 nm, periodicity 141 ± 12 nm, height 75 ± 6 nm) benefited from the co-immobilization of peptides for the enhancement of osteogenic differentiation. Runx2 level for this last functionalization was 3.5 times higher than for non-modified surface, and 1.5 times higher than for the nanostructures functionalized with only one peptide (RGD or BMP-2). COL1A1 expression was similar to the levels observed on plain and RGD-grafted Nanostructures A. Conversely, OCN expression was significantly higher than non-modified nanoarrays for all topographies.

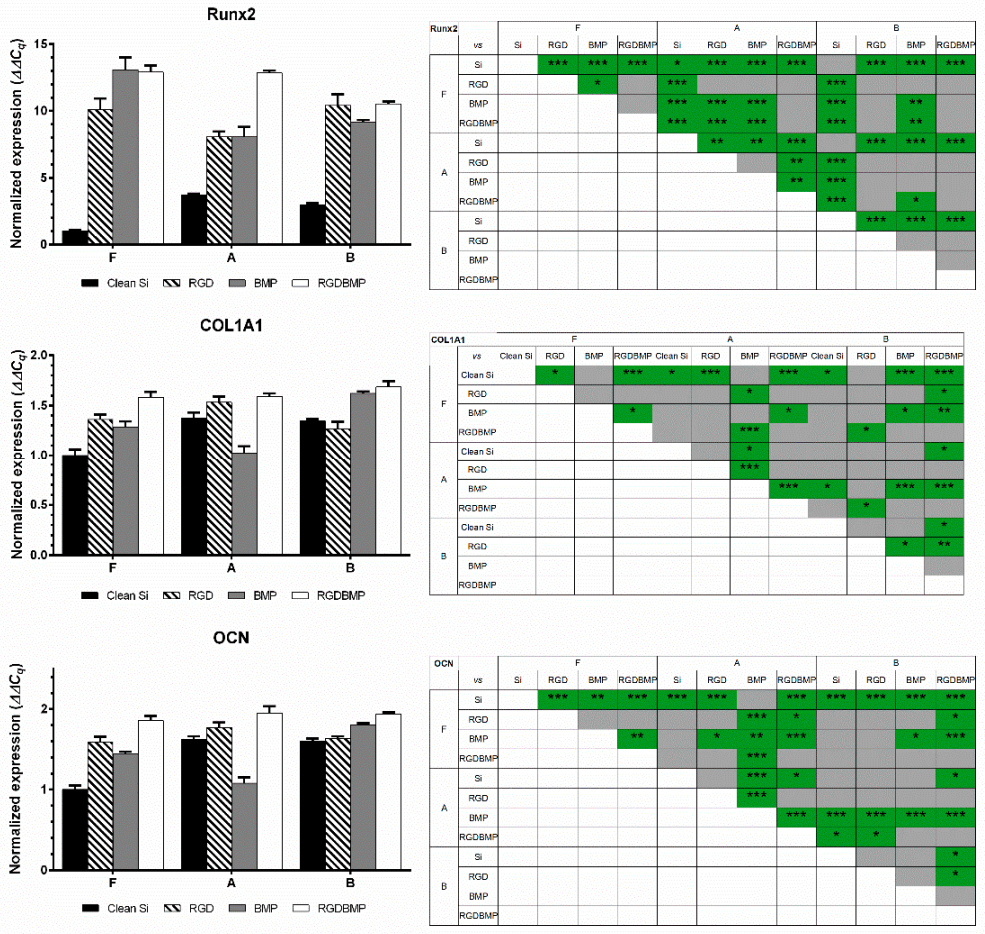

Figure 5. Normalized gene expression from hMSCs cultured for 2 weeks in basal medium, taking non-modified flat silicon as control. Tables summarize significant differences between conditions (grey: non-significant, green: significant differences. * represents $p < 0.05$, ** $p < 0.01$, *** $p < 0.001$).

4. Discussion

Reverse micelles of initial block copolymer (BCPs) granted the possibility of creating ordered polymeric arrays with uniformity over large areas (full wafers) which could be used as masks for the patterning of the underlying substrate with high processing reproducibility. The ability of creating organized nanostructure arrays with high throughput is essential for the subsequent utilization of these samples for cell culture. Such characteristics are essential for the use of silicon nanopillars on studies of hMSC differentiation. A more detailed discussion on this point has been previously reported [18]. XPS characterization showed that surface modification process was successful on the topographies tested. Moreover, since identical atomic % were observed on all surfaces after peptide grafting, it could be concluded that the surface chemistry on all patterns was similar. It was essential to confirm that surface chemistries were homogeneous across a sample area and identical between topographical conditions due to the high sensitivity of hMSCs to small alterations of surface chemistry of a material [34,48].

A uniform distribution of the molecules on the surface was expected on both nanopillar arrays. The theoretical size of unfolded BMP-2 mimetic peptide bound to the surface was ~6 nm, which is less than a fifth of the lowest separation for the array with reduced periodicity (A, 36 nm separation between features). Hence, separation between nanopillars should not result in a preferential distribution of molecules on the nanopatterns. Previous studies demonstrated that cells adhere only to the top part of the pillars when cultured on nanopillar arrays, thus, making molecular distribution on pillar tops to be much more important compared to the inter-feature concavities [49,50]. The top parts of the pillars are

even more accessible for surface-functionalization as compared to a flat surface due to their three-dimensional profiles. Additionally, curvature on the pillar tops is not prominent, with typical rounding radii of 45 nm, which is approximately 10 times larger than the thickness of the molecular layer thickness. Such curvature should not adversely impact the molecular binding to the surface.

hMSCs were cultured for two weeks in basal medium independently of the assay (immunofluorescence or RT-qPCR). Flat and nanopatterned samples were tested right after fabrication or functionalized with RGD or/and BMP-2 mimetic peptide to investigate which could be the best surface for the promotion of osteogenic differentiation of hMSCs.

The nanostructure arrays were selected according to results we previously reported [18]. In that study, modulation of osteogenic differentiation of hMSCs by silicon nanopillar arrays was investigated in vitro. A set of six nanopillar arrays of different dimensions was used as substrates for hMSC culture in basal medium. It was observed that osteogenic differentiation was enhanced for cells cultured on nanopillars of large diameter (100 nm) and height (80 nm). Moreover, it was verified that spacing between features needed to be tuned according to the age of the cell donor to further increase the rate of osteodifferentiation. In agreement with our previous study, after two weeks, non-modified Nanoarray A appeared to be the best surface for the control of hMSC commitment and differentiation towards the osteoblastic lineage, as shown by immunofluorescence and RT-qPCR results [18]. When comparing the expression of the different markers from cells cultured on this pattern with the remaining samples (flat or B), significantly higher levels were observed on Nanotopography A.

Such agreement between immunofluorescence and RT-qPCR results was not verified for biofunctionalized samples. Nonetheless, precise correlations between proteomic and genomic analysis are normally impossible to establish [51,52]. It is necessary to consider protein stability issues, variations in the efficiency of RNA translation, along with possible experimental errors and background noise related to each assay [51,52]. Although cells cultured on non-modified silicon express higher levels of osteogenic markers, and, particularly, markers of late differentiation as OPN, it is necessary to keep into consideration that this is the cell response at two weeks [53]. The observation of RT-qPCR results in more detail indicates that, though osteogenic differentiation may occur slower during the two weeks in culture, it is expected that biofunctionalized surfaces have a significantly higher contribution for the osteoblastic differentiation. The exceptionally high expression of Runx2 on biofunctionalized surfaces (10-fold of the expression observed on bare surfaces), particularly for cells cultured on samples where RGD and BMP-2 peptides were co-immobilized, indicates that a much larger number of cells is starting to differentiate towards the osteoblastic lineage. These trends in marker expression are in agreement with previously reported works [53–56].

Taken together, it is possible to conclude that the impact of surface topography appears to be more effective on the quick modulation of hMSC differentiation than the surface functionalization tested. Considering that Runx2 and COL1A1 are markers of early osteoblast differentiation, whereas OPN and OCN are late markers of differentiation, it can be assumed that Nanopillar Array A (diameter 105 $\pm$ 14 nm, periodicity 141 $\pm$ 12 nm, height 75 $\pm$ 6) is the best nanotopography for the promotion of osteogenesis [53,57]. Though leading to a slower differentiation, co-functionalization of the surfaces, independent of the topography, contributes to a significantly higher expression of the markers studied, hence, to the osteogenic differentiation of a larger fraction of the population. Investigation of the expression of the markers selected at later time points could be of interest towards better understanding of these phenomena.

These results can be of great interest for different in vitro applications. If a large number of differentiated cells is required, then silicon functionalized with RGD and BMP-2 mimetic peptide should be the most suitable option (though undergoing a slower differentiation, a larger fraction of the hMSCs population appears to differentiate when cultured on these bioactive surfaces). Contrarily, if a longer time of storage of the samples before cell

culture is necessary, than non-modified Nanotopography A (small inter-spacing) should be the condition chosen. Non-functionalized samples can potentially be stored indefinitely, which is not the case of samples onto which bioactive molecules were grafted as such molecules have a shorter shelf-life [35].

5. Conclusions

Topographically patterned silicon substrates consisting of silicon nanopillar arrays with well-defined geometric attributes were fabricated on full wafers using self-assembly of block copolymer colloids. Peptides improving adhesion and promoting osteogenic differentiation of hMSCs were successfully grafted onto the silicon nanopillar arrays. Immunofluorescence and RT-qPCR of hMSCs culture on such samples demonstrated that nanostructuring per se can enhance osteoblastic differentiation. Co-immobilization of the two peptides appeared to be an alternative approach to the control of cell differentiation without the need of substrate nanostructuring. These findings suggest that fine-tuning of the surface chemistry and/or topography at nanoscale can modulate cell differentiation without the need of an induction medium. The developed arrays can potentially be used for applications requiring a shorter/longer storage time. Different mimetic peptides could possibly be evaluated in combination of the engineered nanotopographies for a further enhancement of hMSC differentiation. Future main works will provide an assessment of the impact of functionalization, topography, and mechanical properties, including stiffness and viscoelastic behavior, on mesenchymal stem cells differentiation.

Author Contributions: C.R.P. performed the fabrication of the materials with nanopillars, the surface functionalization, the cell culture, the immunofluorescence assays, the RT q-PCR analysis, analyzed data and drafted the manuscript; C.C. supervised the surface functionalization. C.L. performed the XPS analysis and analyzed data; M.-C.D. and S.K. supervised the execution of all experiments and revised the manuscript (equal contribution). All authors have read and agreed to the published version of the manuscript.

Funding: This work was carried out as part of the project EJD-FunMat, which has received funding from the European Union's Horizon 2020 research and innovation program under the Marie Skłodowska-Curie Grant Agreement No. 641640. SK gratefully acknowledges partial funding support of Luxembourg National Research Fund (FNR, Fonds Nationale de la Recherche) via the project PLASENS (C15/MS/10459961).

Acknowledgments: This work was carried out as part of the project EJD-FunMat, which has received funding from the European Union's Horizon 2020 research and innovation program under the Marie Skłodowska-Curie grant agreement No 641640. SK gratefully acknowledges partial funding support of Luxembourg National Research Fund (FNR, Fonds Nationale de la Recherche) via the project PLASENS (C15/MS/10459961), and discussions within COST Action BIONECA. The authors thank Murielle Rémy for the constructive discussions over RT-qPCR and immunofluorescence results, Jerome Guillot for discussion on XPS data, and Didier Arl for help related to SEM data treatment.

Conflicts of Interest: There are no conflicts to declare.

References

1. Williams, D.F. On the nature of biomaterials. *Biomaterials* **2009**, *30*, 5897–5909. [CrossRef]
2. Fraioli, R.; Rechenmacher, F.; Neubauer, S.; Manero, J.M.; Gil, J.; Kessler, H.; Mas-Moruno, C. Mimicking bone extracellular matrix: Integrin-binding peptidomimetics enhance osteoblast-like cells adhesion, proliferation, and differentiation on titanium. *Colloids Surf. B Biointerfaces* **2015**, *128*, 191–200. [CrossRef]
3. Donnelly, H.; Dalby, M.J.; Salmeron-Sanchez, M.; Sweeten, P.E. Current approaches for modulation of the nanoscale interface in the regulation of cell behavior. *Nanomedicine* **2018**, *14*, 2455–2464. [CrossRef] [PubMed]
4. Dalby, M.J.; García, A.J.; Salmeron-Sanchez, M. Receptor control in mesenchymal stem cell engineering. *Nat. Rev. Mater.* **2018**, *3*, 17091. [CrossRef]
5. Metavarayuth, K.; Sitasuwan, P.; Zhao, X.; Lin, Y.; Wang, Q. Influence of Surface Topographical Cues on the Differentiation of Mesenchymal Stem Cells in Vitro. *ACS Biomater. Sci. Eng.* **2016**, *2*, 142–151. [CrossRef] [PubMed]
6. Chen, Z.; Bachhuka, A.; Wei, F.; Wang, X.; Liu, G.; Vasilev, K.; Xiao, Y. Nanotopography-based strategy for the precise manipulation of osteoimmunomodulation in bone regeneration. *Nanoscale* **2017**, *9*, 18129–18152. [CrossRef] [PubMed]

7. Oh, S.; Brammer, K.S.; Li, Y.S.J.; Teng, D.; Engler, A.J.; Chien, S.; Jin, S. Stem cell fate dictated solely by altered nanotube dimension. *Proc. Natl. Acad. Sci. USA* **2009**, *106*, 2130–2135. [CrossRef]
8. Engler, A.J.; Sen, S.; Sweeney, H.L.; Discher, D.E. Matrix Elasticity Directs Stem Cell Lineage Specification. *Cell* **2006**, *126*, 677–689. [CrossRef] [PubMed]
9. Zhou, Q.; Zhao, Z.; Zhou, Z.; Zhang, G.; Chiechi, R.C.; van Rijn, P. Directing Mesenchymal Stem Cells with Gold Nanowire Arrays. *Adv. Mater. Interfaces* **2018**, *5*, 1800334. [CrossRef]
10. Zhang, S.; Ma, B.; Liu, F.; Duan, J.; Wang, S.; Qiu, J.; Li, D.; Sang, Y.; Liu, C.; Liu, D. Polylactic Acid Nanopillar Array-Driven Osteogenic Differentiation of Human Adipose-Derived Stem Cells Determined by Pillar Diameter. *Nano Lett.* **2018**, *18*, 2243–2253. [CrossRef]
11. Su, E.P.; Justin, D.F.; Pratt, C.R.; Sarin, V.K.; Nguyen, V.S.; Oh, S.; Jin, S. Effects of titanium nanotubes on the osseointegration, cell differentiation, mineralisation and antibacterial properties of orthopaedic implant surfaces. *Bone Jt. J.* **2018**, *100*, 9–16. [CrossRef]
12. Sjöström, T.; McNamara, L.E.; Meek, R.M.D.; Dalby, M.J.; Su, B. 2D and 3D nanopatterning of titanium for enhancing osteoinduction of stem cells at implant surfaces. *Adv. Healthc. Mater.* **2013**, *2*, 1285–1293. [CrossRef] [PubMed]
13. McNamara, L.E.; Sjöström, T.; Burgess, K.E.V.; Kim, J.J.W.; Liu, E.; Gordonov, S.; Moghe, P.V.; Meek, R.M.D.; Oreffo, R.O.C.; Su, B.; et al. Skeletal stem cell physiology on functionally distinct titania nanotopographies. *Biomaterials* **2011**, *32*, 7403–7410. [CrossRef]
14. Gui, N.; Xu, W.; Myers, D.E.; Shukla, R.; Tang, H.P.; Qian, M. The effect of ordered and partially ordered surface topography on bone cell responses: A review. *Biomater. Sci.* **2018**, *6*, 250–264. [CrossRef] [PubMed]
15. Dalby, M.J.; Gadegaard, N.; Oreffo, R.O.C. Harnessing nanotopography and integrin–matrix interactions to influence stem cell fate. *Nat. Mater.* **2014**, *13*, 558–569. [CrossRef]
16. Vining, K.H.; Mooney, D.J. Mechanical forces direct stem cell behaviour in development and regeneration. *Nat. Rev. Mol. Cell Biol.* **2017**, *18*, 728–742. [CrossRef]
17. Kim, M.; Kim, C.; Choi, Y.S.; Kim, M.; Park, C.; Suh, Y. Age-related alterations in mesenchymal stem cells related to shift in differentiation from osteogenic to adipogenic potential: Implication to age-associated bone diseases and defects. *Mech. Ageing Dev.* **2012**, *133*, 215–225. [CrossRef]
18. Pedrosa, C.R.; Arl, D.; Grysan, P.; Khan, I.; Durrieu, S.; Krishnamoorthy, S.; Durrieu, M.C. Controlled Nanoscale Topographies for Osteogenic Differentiation of Mesenchymal Stem Cells. *ACS Appl. Mater. Interfaces* **2019**, *11*, 8858–8866. [CrossRef] [PubMed]
19. Mas-Moruno, C. Surface functionalization of biomaterials for bone tissue regeneration and repair. In *Peptides and Proteins as Biomaterials for Tissue Regeneration and Repair*, 1st ed.; Barbosa, M.A., Martins, M.C.L., Eds.; Elsevier: Amsterdam, The Netherlands, 2018; pp. 73–100.
20. Mas-Moruno, C.; Fraioli, R.; Rechenmacher, F.; Neubauer, S.; Kapp, T.G.; Kessler, H. αvβ3- or α5β1-Integrin-Selective Peptidomimetics for Surface Coating. *Angew. Chem. Int. Ed. Engl.* **2016**, *55*, 7048–7067. [CrossRef]
21. Ratner, B.D.; Hoffman, A.S.; Schoen, F.J.; Lemons, J.E. *Biomaterials Science: An Introduction to Materials in Medicine*; Elsevier Academic Press: Amsterdam, The Netherlands; Boston, MA, USA; Paris, France, 2004.
22. Carvalho, M.S.; Cabral, J.M.S.; da Silva, C.L.; Vashishth, D. Bone Matrix Non-Collagenous Proteins in Tissue Engineering: Creating New Bone by Mimicking the Extracellular Matrix. *Polymers* **2021**, *13*, 1095. [CrossRef]
23. Curry, A.S.; Pensa, N.W.; Barlow, A.M.; Bellis, S.L. Taking cues from the extracellular matrix to design bone-mimetic regenerative scaffolds. *Matrix Biol.* **2016**, *52–54*, 397–412. [CrossRef]
24. Carvalho, M.S.; Silva, J.C.; Hoff, C.M.; Cabral, J.M.S.; Linhardt, R.J.; da Silva, C.L.; Vashishth, D. Loss and rescue of osteocalcin and osteopontin modulate osteogenic and angiogenic features of mesenchymal stem/stromal cells. *J. Cell. Physiol.* **2020**, *235*, 7496–7515. [CrossRef] [PubMed]
25. Klimek, K.; Ginalska, G. Proteins and Peptides as Important Modifiers of the Polymer Scaffolds for Tissue Engineering Applications-A Review. *Polymers* **2020**, *12*, 844. [CrossRef]
26. Collier, J.H.; Segura, T. Evolving the use of peptides as components of biomaterials. *Biomaterials* **2011**, *32*, 4198–4204. [CrossRef] [PubMed]
27. Porté-Durrieu, M.C.; Guillemot, F.; Pallu, S.; Labrugère, C.; Brouillaud, B.; Bareille, R.; Amédée, J.; Barthe, N.; Dard, M.; Baquey, C. Cyclo-(DfKRG) peptide grafting onto Ti-6Al-4V: Physical characterization and interest towards human osteoprogenitor cells adhesion. *Biomaterials* **2004**, *25*, 4837–4846. [CrossRef] [PubMed]
28. Cheng, Z.A.; Zouani, O.F.; Glinel, K.; Jonas, A.M.; Durrieu, M.C. Bioactive chemical nanopatterns impact human mesenchymal stem cell fate. *Nano Lett.* **2013**, *13*, 4996. [CrossRef]
29. Bellis, S.L. Advantages of RGD peptides for directing cell association with biomaterials. *Biomaterials* **2011**, *32*, 4205–4210. [CrossRef]
30. Schwab, E.H.; Pohl, T.L.M.; Haraszti, T.; Schwaerzer, G.K.; Hiepen, C.; Spatz, J.P.; Knaus, P.; Cavalcanti-Adam, E.A. Nanoscale control of surface immobilized BMP-2: Toward a quantitative assessment of BMP-mediated signaling events. *Nano Lett.* **2015**, *15*, 1526–1534. [CrossRef] [PubMed]
31. Migliorini, E.; Valat, A.; Picart, C.; Cavalcanti-Adam, E.A. Tuning cellular responses to BMP-2 with material surfaces. *Cytokine Growth Factor Rev.* **2016**, *27*, 43–54. [CrossRef]
32. Zouani, O.F.; Rami, L.; Lei, Y.; Durrieu, M.C. Insights into the osteoblast precursor differentiation towards mature osteoblasts induced by continuous BMP-2 signaling. *Biol. Open* **2013**, *2*, 872–881. [CrossRef] [PubMed]

33. Kim, M.J.; Lee, B.; Yang, K.; Park, J.; Jeon, S.; Um, S.H.; Kim, D.I.; Im, S.G.; Cho, S.W. BMP-2 peptide-functionalized nanopatterned substrates for enhanced osteogenic differentiation of human mesenchymal stem cells. *Biomaterials* **2013**, *34*, 7236–7246. [CrossRef] [PubMed]
34. Padiolleau, L.; Chanseau, C.; Durrieu, S.; Chevallier, P.; Laroche, G.; Durrieu, M.C. Single or mixed tethered peptides to promote hMSC differentiation toward osteoblastic lineage. *ACS Appl. Bio Mater.* **2018**, *1*, 1800–1809. [CrossRef]
35. Bilem, I.; Chevallier, P.; Plawinski, L.; Sone, E.D.; Durrieu, M.C.; Laroche, G. RGD and BMP-2 mimetic peptide crosstalk enhances osteogenic commitment of human bone marrow stem cells. *Acta Biomater.* **2016**, *36*, 132–142. [CrossRef] [PubMed]
36. Bilem, I.; Chevallier, P.; Plawinski, L.; Sone, E.D.; Durrieu, M.C.; Laroche, G. Interplay of Geometric Cues and RGD/BMP-2 Crosstalk in Directing Stem Cell Fate. *ACS Biomater. Sci. Eng.* **2017**, *3*, 2514–2523. [CrossRef]
37. Ma, Y.; Policastro, G.M.; Li, Q.; Zheng, J.; Jacquet, R.; Landis, W.J.; Becker, M.L. Concentration-Dependent hMSC Differentiation on Orthogonal Concentration Gradients of GRGDS and BMP-2 Peptides. *Biomacromolecules* **2016**, *17*, 1486–1495. [CrossRef]
38. Zouani, O.F.; Chollet, C.; Guillotin, B.; Durrieu, M.C. Differentiation of pre-osteoblast cells on poly(ethylene terephthalate) grafted with RGD and/or BMPs mimetic peptides. *Biomaterials* **2010**, *31*, 8245–8253. [CrossRef]
39. Kaur, G.; Wang, C.; Sun, J.; Wang, Q. The Synergistic Effects of Multivalent Ligand Display and Nanotopography on Osteogenic Differentiation of Rat Bone Marrow Stem Cells. *Biomaterials* **2010**, *31*, 5813–5824. [CrossRef]
40. Lai, M.; Jin, Z.; Su, Z. Surface modification of TiO 2 nanotubes with osteogenic growth peptide to enhance osteoblast differentiation. *Mater. Sci. Eng. C* **2017**, *73*, 490–497. [CrossRef] [PubMed]
41. Gao, X.; Zhang, X.; Song, J.; Xu, X.; Xu, A.; Wang, M.; Xie, B.; Huang, E.; Deng, F.; Wei, S. Osteoinductive peptide-functionalized nanofibers with highly ordered structure as biomimetic scaffolds for bone tissue engineering. *Int. J. Nanomed.* **2015**, *10*, 7109.
42. Krishnamoorthy, S.; Manipaddy, K.K.; Yap, F.L. Wafer-Level Self-Organized Copolymer Templates for Nanolithography with Sub-50 nm Feature and Spatial Resolutions. *Adv. Funct. Mater.* **2011**, *21*, 1102–1112. [CrossRef]
43. Cunha, A.; Zouani, O.F.; Plawinski, L.; Botelho do Rego, A.M.; Almeida, A.; Vilar, R.; Durrieu, M.C. Human mesenchymal stem cell behavior on femtosecond laser-textured Ti-6Al-4V surfaces. *Nanomedicine* **2015**, *10*, 725–739. [CrossRef] [PubMed]
44. Bilem, I.; Plawinski, L.; Chevallier, P.; Ayela, C.; Sone, E.D.; Laroche, G.; Durrieu, M.C. The spatial patterning of RGD and BMP-2 mimetic peptides at the subcellular scale modulates human mesenchymal stem cells osteogenesis. *J. Biomed. Mater. Res. A* **2018**, *106*, 959–970. [CrossRef]
45. Zouani, O.F.; Kalisky, J.; Ibarboure, E.; Durrieu, M.C. Effect of BMP-2 from matrices of different stiffnesses for the modulation of stem cell fate. *Biomaterials* **2013**, *34*, 2157–2166. [CrossRef]
46. Inoue, M.; Shinohara, M.L. Intracellular osteopontin (iOPN) and immunity. *Immunol. Res.* **2011**, *49*, 160–172. [CrossRef]
47. Pfaffl, M.W.; Tichopad, A.; Prgomet, C.; Neuvians, T.P. Determination of stable housekeeping genes, differentially regulated target genes and sample integrity: BestKeeper—Excel-based tool using pair-wise correlations. *Biotechnol. Lett.* **2004**, *26*, 509–515. [CrossRef] [PubMed]
48. Phillips, J.E.; Petrie, T.A.; Creighton, F.P.; García, A.J. Human mesenchymal stem cell differentiation on self-assembled monolayers presenting different surface chemistries. *Acta Biomater.* **2010**, *6*, 12–20. [CrossRef] [PubMed]
49. De Peppo, G.M.; Agheli, H.; Karlsson, C.; Ekström, K.; Brisby, H.; Lennerås, M.; Gustafsson, S.; Sjövall, P.; Johansson, A.; Olsson, E.; et al. Osteogenic response of human mesenchymal stem cells to well-defined nanoscale topography in vitro. *Int. J. Nanomed.* **2014**, *9*, 2499–2515. [CrossRef]
50. Fiedler, J.; Özdemir, B.; Bartholomä, J.; Plettl, A.; Brenner, R.E.; Ziemann, P. The effect of substrate surface nanotopography on the behavior of multipotnent mesenchymal stromal cells and osteoblasts. *Biomaterials* **2013**, *34*, 8851–8859. [CrossRef]
51. Vogel, C.; Marcotte, E.M. Insights into the regulation of protein abundance from proteomic and transcriptomic analyses. *Nat. Rev. Genet.* **2012**, *13*, 227–232. [CrossRef]
52. Maier, T.; Güell, M.; Serrano, L. Correlation of mRNA and protein in complex biological samples. *FEBS Lett.* **2009**, *583*, 3966–3973. [CrossRef]
53. Miron, R.J.; Zhang, Y.F. Osteoinduction: A review of old concepts with new standards. *J. Dent. Res.* **2012**, *91*, 736–744. [CrossRef] [PubMed]
54. Sun, M.; Chi, G.; Li, P.; Lv, S.; Xu, J.; Xu, Z.; Xia, Y.; Tan, Y.; Xu, J.; Li, L. Effects of Matrix Stiffness on the Morphology, Adhesion, Proliferation and Osteogenic Differentiation of Mesenchymal Stem Cells. *Int. J. Med. Sci.* **2018**, *15*, 257. [CrossRef]
55. Chen, X.; Sun, X.; Yang, X.; Zhang, L.; Lin, M.; Yang, G.; Gao, C.; Feng, Y.; Yu, J.; Gou, Z. Biomimetic preparation of trace element-codoped calcium phosphate for promoting osteoporotic bone defect repair. *J. Mater. Chem. B* **2013**, *1*, 1316–1325. [CrossRef] [PubMed]
56. Vimalraj, S.; Arumugam, B.; Miranda, P.J.; Selvamurugan, N. Runx2: Structure, function, and phosphorylation in osteoblast differentiation. *Int. J. Biol. Macromol.* **2015**, *78*, 202–208. [CrossRef] [PubMed]
57. Alberts, B.; Johnson, A.; Lewis, J.; Raff, M.; Roberts, K.; Walter, P. *Molecular Biology of the Cell*, 4th ed.; Garland Science: New York, NY, USA, 2002; pp. 1227–1242.